INVESTIGATIONS OF CONTINUOUS BED LOAD SALTATING PROCESS

By Hong-Yuan Lee,[1] Member, ASCE, Yen-Hsu Chen,[2] Jiing-Yun You,[3] and Ying-Tien Lin[4]

ABSTRACT: Particle saltating motions during bed load transport are dominated by the forces acting upon particles and the random process of the particles impacting on and rebounding from the channel bed. A real-time flow visualization technique is developed in this study to measure particle saltating trajectories, corresponding velocities, and impacting and rebounding angles. Based on the experimental data, regression equations for the dimensionless saltating length, height, and velocity were obtained. A numerical model that is able to simulate the continuous saltating process of a single particle was developed. The model was calibrated and verified with the experimental data, and the results were satisfactory. The model was also used to generate a series of synthetic data. Based on these data and the flume data collected by previous investigators, a bed load equation was derived.

INTRODUCTION

Sediment transport in water can generally be classified into two major modes, namely, bed load and suspended load. The mode of transport depends on the size of the bed materials and the flow conditions. When the bed-shear stress exceeds the critical value for initiation of motion, a grain begins to move by sliding or rolling over the bed. If the bed-shear stress further increases, these particles will hop up from the bed and start to saltate. The transport of particles by rolling, sliding, and saltating is called bed load transport, and this is the subject investigated in this study. According to the previous investigations, the bulk of bed load transport occurs in the saltation mode (Einstein 1942; Sekine and Kikkawa 1992; Wiberg and Smith 1987, 1989), and the kinematic characteristics of saltation are dominated by the flow conditions, size of the saltating particles, and the random process of the particle impacting on and rebounding from the channel bed. Hence, investigations of the continuous saltation is crucial to the study of bed load transport.

Numerous researchers have investigated the saltating process. Based on his flume study, Einstein (1950) found the thickness of the bed load transport is about two times the particle size, and the saltation length is about 100 times the particle size. Gordon et al. (1972), Francis (1973), Abbott and Francis (1977), and Murphy and Hooshiari (1982) used a multiple-exposure technique to measure the saltating trajectories and the corresponding velocities of a saltating particle in water. However, due to the limitation of the technique used, the particles have to be larger than 3 mm. Van Rijn (1984) established a single-step saltating model. This model was calibrated and verified with the data collected by previously mentioned researchers and is applicable to low Reynolds number flows. Wiberg and Smith (1985) established a continuous saltation numerical model. In this model, a 2D impacting and rebounding scheme was proposed. The friction coefficient was assumed to be equal to the restitution coefficient, and this coefficient was used as the calibration factor. Hui and Hu (1991) used a high-speed photographic technique to measure the particle motions near the channel bed and proposed the dividing boundaries between rolling, saltating, sliding, and suspending motions. Sekine and Kikkawa (1992) assumed the position of the sediment particles in the channel bed followed a Gaussian distribution and adopted the stochastic theory and random number generation model to develop a 3D impacting and rebounding model. The friction and restitution coefficients were assumed equal in their model. Nino and Garcia (1994, 1998) also developed a high-speed photographic technique to measure the saltation trajectories and established a 2D continuous saltation model. Lee and Hsu (1994) developed a real-time photographic technique and a high-speed photographic technique to measure the saltation trajectories and the corresponding velocities. They also established a single-step saltation model, and the model was calibrated and verified with the laboratory data.

EXPERIMENTAL SETUP

The experiments were conducted in a 12-m-long × 0.3-m-wide slope-adjustable recirculating flume. Several combinations of water depth, channel slope, particle size, and specific gravity for the particles were tested. The water depth was fixed at 5 cm, and the range of the slope was from 0.003 to 0.008. Particles with a diameter of 0.6 cm and specific gravities of 1.38 and 1.08 were chosen. Particles of the same size as for the saltating particles were glued to the channel bed. Key hydraulic and sediment transport characteristics are given in Table 1, where u_* is the shear velocity, u_{*c} is the critical shear velocity, and θ is the dimensionless shear stress.

The real-time flow visualization system consists of a CV-M30 charged-coupled device (CCD) camera, a Nikon 35-mm lenz, an IBM PC 586, and a Coreco F64 professional image-processing card. The system can take 30 photos, 512 × 512 pixels/s and then transfers the photos into digitized formats through an Optimus V5.22 image processing software. The general configuration of the experimental setup is shown in Fig. 1. During the experimental process, the laboratory was kept in complete darkness, and the only light sources were installed at both sides of the CCD camera. Sediment particles were released at about 2-m upstream of the working section. As the saltating particles passed through the working section, the images were recorded by the CCD camera.

The analogical images were transferred into digitized images, with 256 different gray levels, through an analog-to-digital convertor and then stored in a video ram of an F64 pro image-processing card installed in an IBM PC 586. The digitized images were analyzed using an Optimas V5.22 software. The background noises were first eliminated through a logical subtract process to outshine the particle images. The area and the centroid of the images were then calculated to identify the locations of the particles and then transmitted into a worktable through a data dynamic exchange process. Be-

[1]Prof., Dept. of Civ. Engrg., Nat. Taiwan Univ., Taipei 10764, Taiwan.
[2]Grad. Res. Asst., Dept. of Civ. Engrg., Nat. Taiwan Univ., Taipei 10764, Taiwan.
[3]Grad. Res. Asst., Dept. of Civ. Engrg., Nat. Taiwan Univ., Taipei 10764, Taiwan.
[4]Grad. Res. Asst., Dept. of Civ. Engrg., Nat. Taiwan Univ., Taipei 10764, Taiwan.

Note. Discussion open until February 1, 2001. To extend the closing date one month, a written request must be filed with the ASCE Manager of Journals. The manuscript for this paper was submitted for review and possible publication on June 28, 1999. This paper is part of the ***Journal of Hydraulic Engineering***, Vol. 126, No. 9, September, 2000. ©ASCE, ISSN 0733-9429/00/0009-0691–0700/$8.00 + $.50 per page. Paper No. 21284.

TABLE 1. Experimental Data

Run (1)	Trajectory numbers (2)	Particle Size D (cm) (3)	Particle Specific weight ρ_s (4)	Water depth H (cm) (5)	Slope S_0 (6)	u_* (cm/s) (7)	u_{*c} (cm/s) (8)	θ (9)	Mean flow velocity (cm/s) (10)
C-01	36	0.6	1.38	5.0	0.004	3.84	3.66	0.066	54.4
C-02	70	0.6	1.38	5.0	0.006	4.70	3.66	0.099	65.0
C-03	56	0.6	1.38	5.0	0.008	5.42	3.66	0.131	73.3
C-04	143	0.6	1.08	5.0	0.003	3.32	1.68	0.234	48.5
C-05	71	0.6	1.08	5.0	0.005	4.29	1.68	0.391	60.3
C-06	56	0.6	1.08	5.0	0.007	5.07	1.68	0.546	70.0

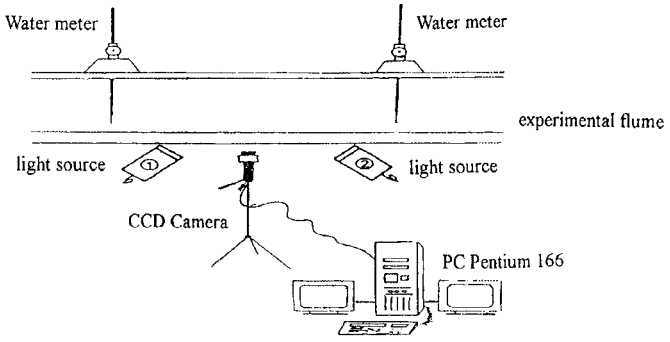

FIG. 1. Layout of Experimental Setup

cause the time interval between the images taken was fixed, the instantaneous saltating velocity vector can thus be obtained. A typical trajectory is shown in Fig. 2.

DIMENSIONAL ANALYSIS

The parameters that affect the particle saltating motions include water depth H, channel slope S_0, specific gravity of water ρ_w, dynamic viscosity μ, saltating particle size D, size of the particles that form the channel bed D_b, specific gravity of the saltating particle ρ_s, particle surface roughness ε, and gravitational acceleration g. Using Buckingham's π method, the following dimensionless equation can be obtained:

$$\hat{F} = f_1\left(\theta, \mathsf{R}_*, \frac{H}{D}, \frac{D_b}{D}, \frac{\varepsilon}{D_b}, \frac{\rho_s}{\rho_w}\right) \tag{1}$$

where $\hat{F}$ = dimensionless saltating characteristics, including saltation height, length, and velocity; $\theta = \rho_w u_*^2/g(\rho_s - \rho_w)D$ = dimensionless shear stress; $u_* = (S_0 gH)^{1/2}$ = shear velocity; and $\mathsf{R}_* = u_* D/\nu$ = particle Reynolds number. Because $H >> D$, $D_b >> \varepsilon$, and $D_b = D$, these three terms can be discarded in (1). Combining θ and R_* and eliminating u_*, a dimensionless parameter $D_* = D[(S_G - 1)g/\nu^2]^{1/3}$ can be obtained, where $S_G = \rho_s/\rho_w$.

Replacing u_* with $(u_* - u_{*c})$, θ can be transferred into $T_* = (u_*^2 - u_{*c}^2)/u_{*c}^2$. Eq. (1) can therefore be simplified to

$$\hat{F} = f_2(T_*, D_*) \tag{2}$$

THEORETICAL MODEL

The forces acting on saltating particles include inertia force, submerged weight, virtual mass effect force, lift force, and drag force. Applying Newton's second law, the equation of motion of the saltating particles are

$$m\ddot{x} = F_L\left(\frac{\dot{z}}{u_r}\right) + F_D\left(\frac{u - \dot{x}}{u_r}\right) + F_G \sin\phi \tag{3}$$

$$m\ddot{z} = F_L\left(\frac{u - \dot{x}}{u_r}\right) - F_D\left(\frac{\dot{z}}{u_r}\right) - F_G \cos\phi \tag{4}$$

where $m = (\rho_s + C_m\rho_w)\pi D^3/6$ = particle total mass; C_m = virtual mass coefficient and is assumed to be 0.5 (Wiberg and Smith 1985) in this model; $\dot{x}$, $\dot{z}$, $\ddot{x}$, and $\ddot{z}$ represent the longitudinal and vertical components of particle velocity and acceleration, respectively; $u_r = \sqrt{(\dot{x} - u)^2 + \dot{z}^2}$ = relative velocity; ϕ = channel-bed angle; $F_G = \alpha_1(\rho_s - \rho_w)gD^3$ = submerged weight; F_L = lift force; and F_D = drag force. The formulations of F_L and F_D are given below.

Drag force is caused by a combination of pressure difference and skin friction. It is expressed as

$$F_D = C_D \beta D^2 \frac{\rho_w u_r^2}{2} \tag{5}$$

where C_D = drag coefficient; and βD^2 = projected area perpendicular to the flow direction. The drag coefficients can be expressed by the empirical relation of Swamee and Ojha (1991)

$$C_D = 0.5\left\{16\left[\left(\frac{24}{\mathsf{R}}\right)^{1.6} + \left(\frac{130}{\mathsf{R}}\right)^{0.72}\right]^{2.5} + \left[\left(\frac{40{,}000}{\mathsf{R}}\right)^2 + 1\right]^{-0.25}\right\}^{0.25} \tag{6}$$

where R = Reynolds number (i.e., $\mathsf{R} = uD/\nu$, where ν is the viscosity).

Several different formulas are available for calculating the lift force. The one proposed by Anderson and Hallet (1986) is used in this study

$$F_L = \frac{1}{2}\rho_w A C_L(u_{rT}^2 - u_{rB}^2) \tag{7}$$

where u_{rT} and u_{rB} = relative velocities at the top and bottom of the particle, respectively; A = cross-sectional area of the particle perpendicular to the flow direction; and C_L = lift coefficient. The lift coefficient is affected by the particle size, shape, spinning velocity, and flow field. It is generally treated as a constant to be calibrated (Wiberg and Smith 1985).

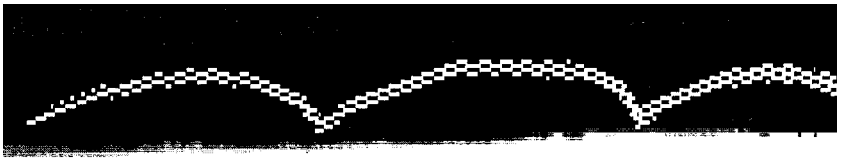

FIG. 2. Typical Saltating Trajectory

IMPACTING AND REBOUNDING MECHANISM

A model that is able to reflect the impacting and rebounding process is crucial to the simulation of a continuous saltating process. The model proposed by Nino and Garcia (1994) was adopted in this study. The model is described in Appendix I.

INITIAL CONDITIONS

The initial position of the particle was assumed to be $0.6D$ from the average channel bed (Van Rijn 1984), and the initial longitudinal and vertical components of the liftoff velocity were assumed to be $\alpha_1 u_*$ and $\alpha_2 u_*$, which are to be calibrated.

NUMERICAL SOLUTION TECHNIQUE

The governing equations [(3) and (4)] are second-order nonlinear partial differential equations. They were transformed into a system of first-order ordinary differential equations and then solved by Runge-Kutta and Gill methods.

The coefficients calibrated in the model include the lift coefficient C_L, restitution coefficient e, friction coefficient f, and

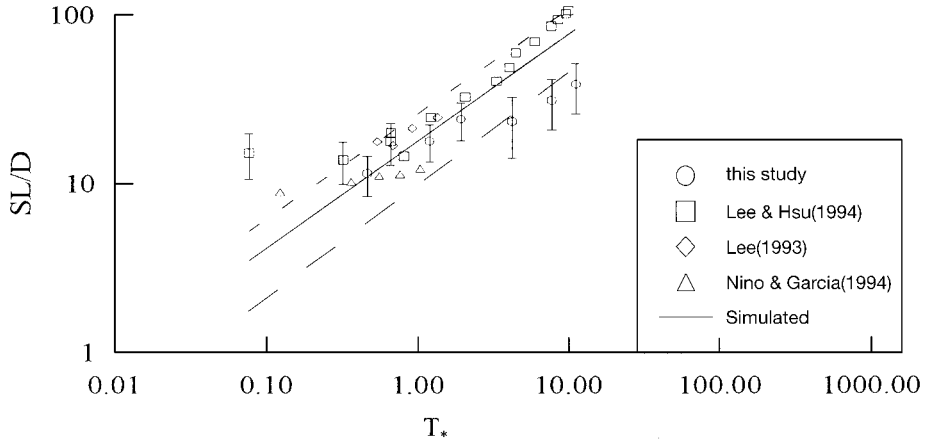

FIG. 3. Relations between Simulated and Dimensionless Saltating Length and T_*

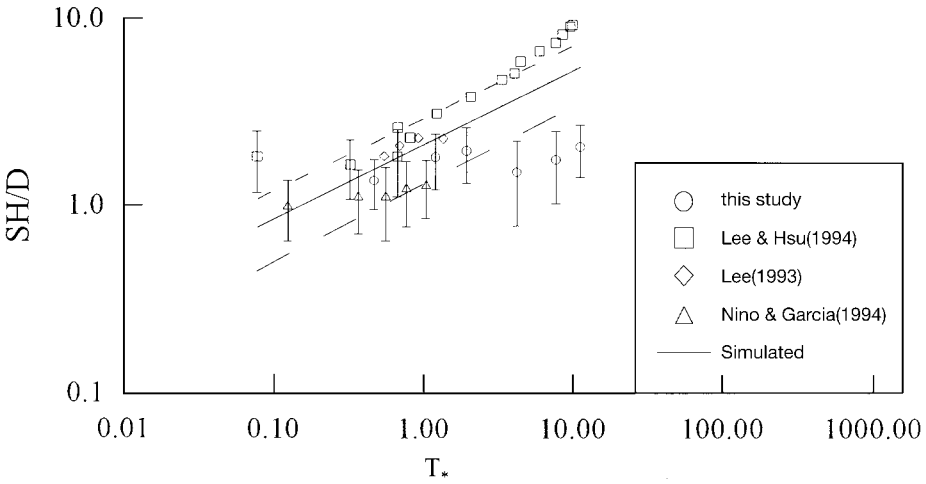

FIG. 4. Relations between Simulated and Dimensionless Saltating Height and T_*

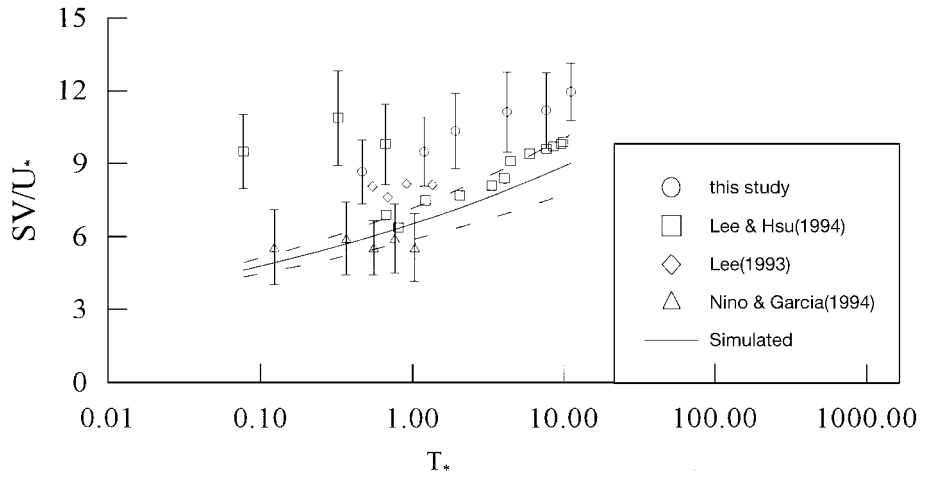

FIG. 5. Relations between Simulated Dimensionless Saltating Velocity and T_*

the initial longitudinal and vertical components of the liftoff velocity $\alpha_1 u_*$ and $\alpha_2 u_*$, respectively. Fifty-five continuous saltating trajectories were simulated by the model. By comparing the averaged saltating characteristics (including heights, lengths, and velocities) with the experimental data collected in this study and also with those of Lee (1993), Nino and Garcia (1994), and Lee and Hsu (1994), the above-mentioned coefficients were calibrated to be $\alpha_1 = \alpha_2 = 2.5$, $C_L = 4.6$, $e = 0.31$, and $f = 0.92$. The relations between the simulated saltating length, height, and velocity and T_* are shown in Figs. 3–5, respectively. The two dotted lines above and below the simulated curve represent one standard deviation above and below the simulation results, respectively. Many factors including turbulent eddy, turbulent bursting, particle rotating, and wall effects are not considered in the model, and this may explain the deviations observed in Figs. 3–5.

RESULTS AND DISCUSSIONS

Experimental Results

There was a total of 432 trajectories recorded, the relations between measured dimensionless saltating length, height, velocity, location of the peak of the saltating trajectory, and incidence and takeoff angles are shown in Figs. 6–10, respectively. The saltating length is about 11.7–38.3 times particle size, the saltating height is about 1.35–2.05 times particle size, the average saltating velocity is about 9–10.6 times shear velocity, the averaged takeoff angle is between 20° and 29°, the averaged incidence angle is between 9° and 12°, and the peak of the saltating trajectory is located at about 40% of the total saltating displacement. Saltating length, height, and velocity increase with the flow intensity, whereas the incidence and takeoff angles and location of the peak vary inversely with the flow intensity. Averaged dimensionless saltating length and height were observed to follow Pearson Type III distributions, and dimensionless saltating velocity follows a normal distribution. These distribution curves are shown in Fig. 11. The distribution curves of incidence and takeoff angles are shown in Fig. 12. And rebounding angles θ_r is shown in Fig. 13, where the incidence and takeoff angles were directly measured from the experiments and the rebounding angles were calculated using the Collision-rebound model of Nino and Garcia (1994). The variance of takeoff angle is about two times of that of incidence angles. The distribution curves of takeoff angles under various incidence conditions are shown in Fig. 14. It shows that takeoff angles are not significantly related to incidence angles. This supports the randomness assumption for incidence and takeoff schemes used in this model.

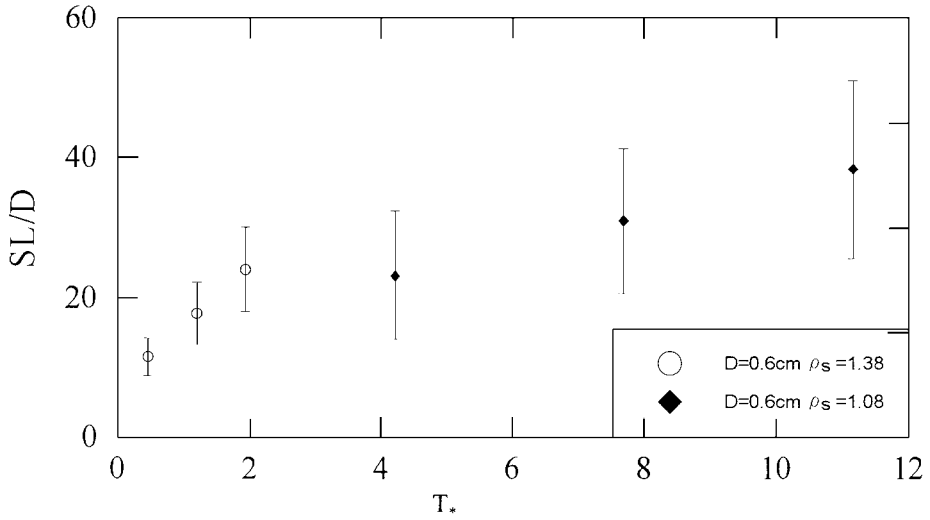

FIG. 6. Relations between Measured Dimensionless Saltating Length and T_*

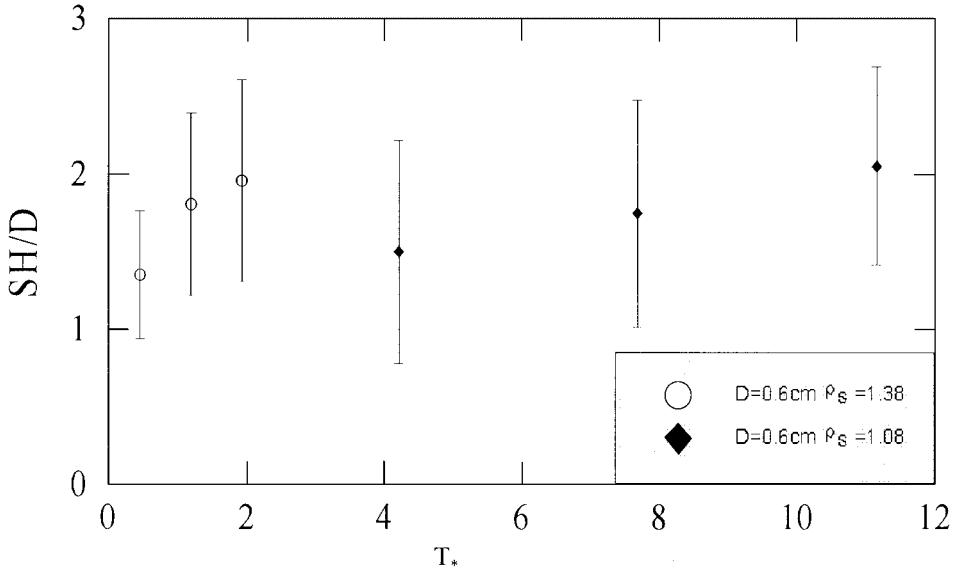

FIG. 7. Relations between Measured Dimensionless Saltating Height and T_*

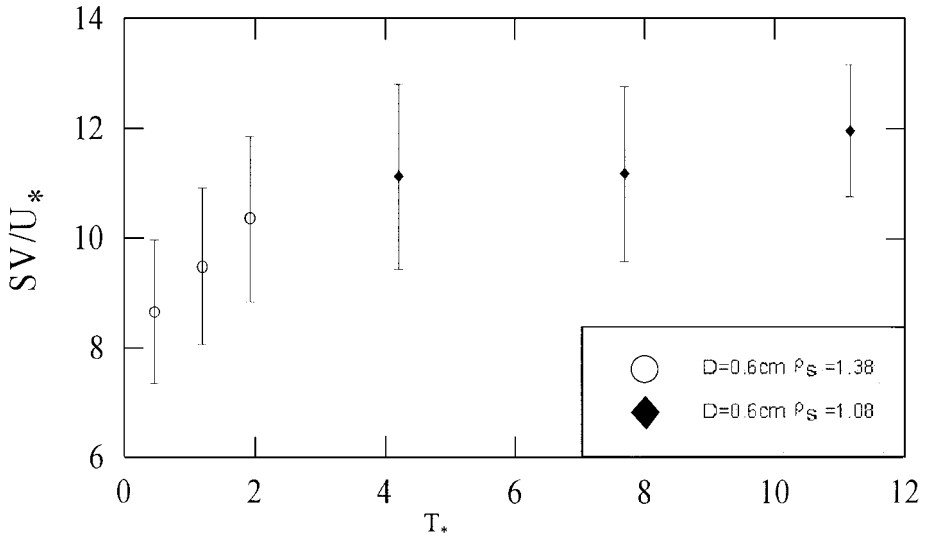

FIG. 8. Relations between Measured Dimensionless Saltating Velocity and T_*

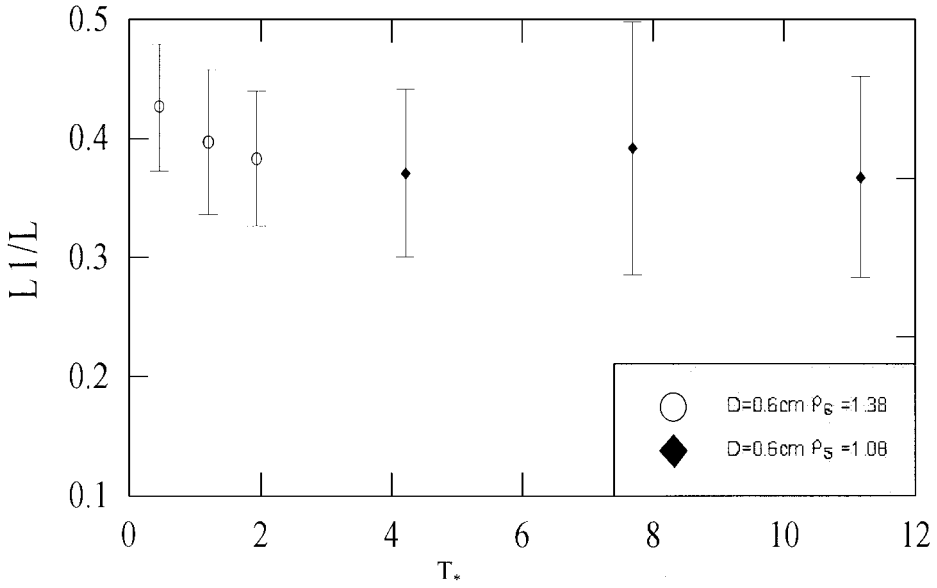

FIG. 9. Relations between Location of Peak of Saltating Trajectory and T_* (L Is Saltating Length and $L1$ Is Distance When Saltating Particle Reaches Maximum Height)

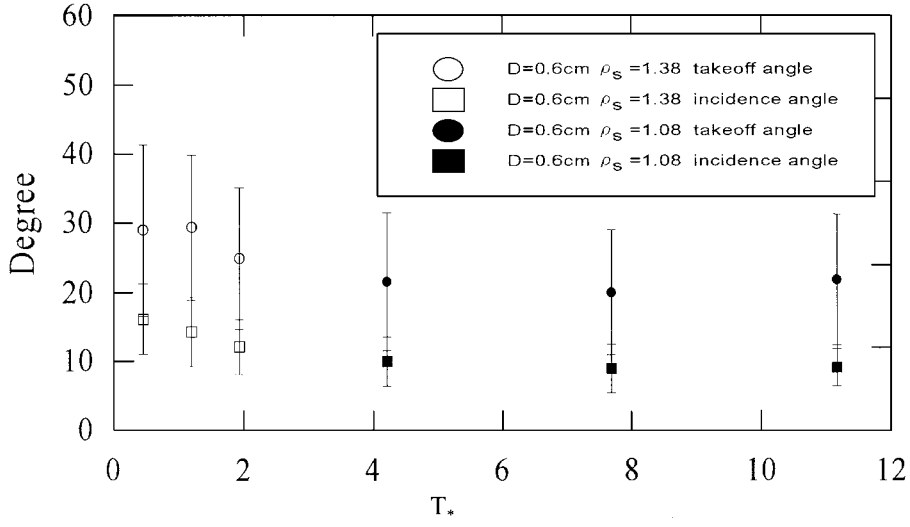

FIG. 10. Relations between Incidence and Takeoff Angles and T_*

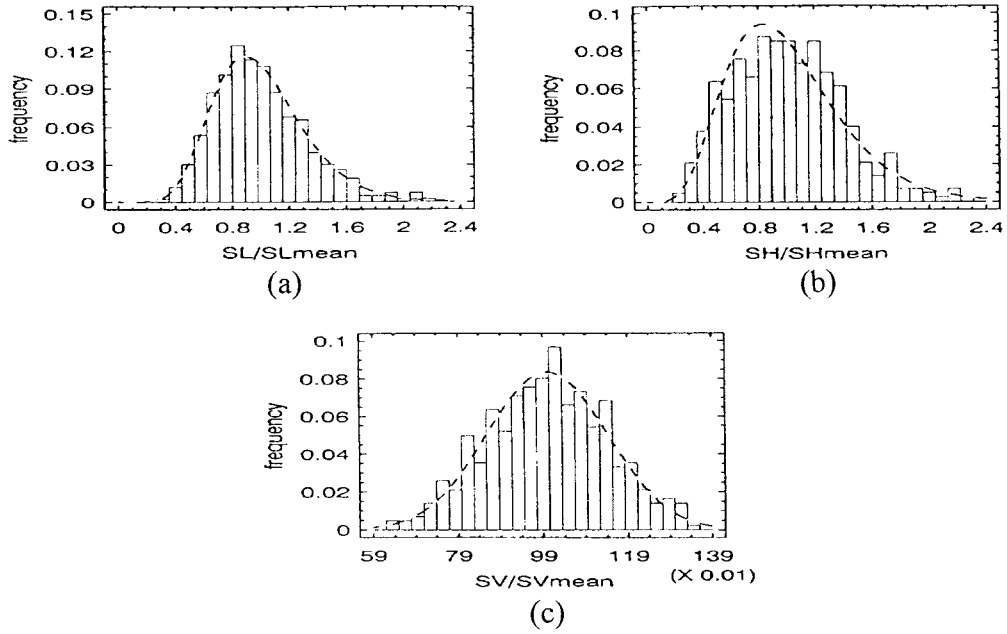

FIG. 11. Distributions of: (a) Measured Dimensionless Saltating Lengths; (b) Heights; (c) Velocities

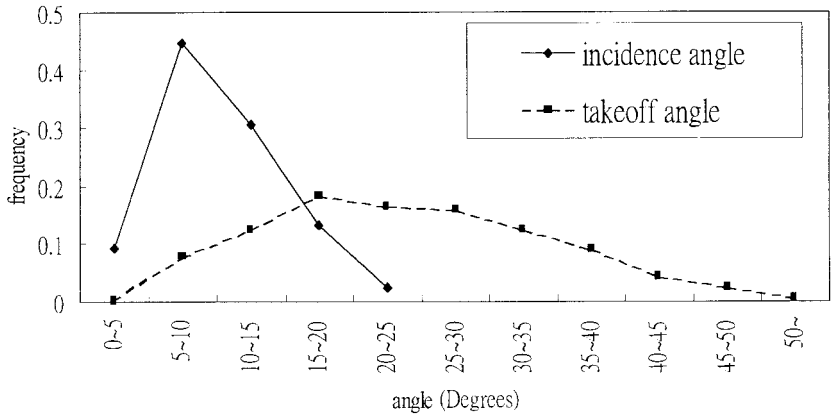

FIG. 12. Distributions of Incidence Angles θ_{in} and Takeoff Angles θ_{out}

Numerical Simulation Results

The numerical model was applied to simulate the continuous saltating trajectories under 60 different combinations, including six particle sizes and 10 flow conditions. A typical trajectory is shown in Fig. 15. It was found that dimensionless saltating length SL/D increases as D_* increases. However, when T_* is large, the increment is not significant. This indicates that the variations of the dimensionless saltating length are not significant to the particle sizes under strong flow conditions. Einstein (1942) and Einstein and El-Sammi (1949) pointed out that saltating length is only affected by particle size and shape and has nothing to do with the flow condition. Our simulation results verified Einstein's proposition but only under a strong flow condition. Under low flow conditions, saltating length is dependent on the flow condition.

It is also found that dimensionless saltating height SH/D increases as T_* and D_* increase. When T_* is small, SV/U_* increases with D_*. However, when T_* is large, variations of SV/U_* are not significant compared to the variations of D_*, especially when the D_* value is large. The explanation is the same as that for the dimensionless saltating height.

It is also found that lift forces are larger than drag forces in the saltating processes of large particles. Magnitudes of these two forces are close when saltating particles are small. This again further explains the phenomena discussed above.

Simulated incidence and takeoff angles from the model are shown in Fig. 16, which shows that the variations of the incidence angles are larger than those of the takeoff angles. These variations are closely related to the particle sizes but not sensitive to the flow intensities.

The frequency histograms of the simulated SL/SL_{mean}, SH/SH_{mean}, and SV/SV_{mean} are shown in Fig. 17, in which SL_{mean}, SH_{mean}, and SV_{mean} represent mean saltating length, height, and velocity, respectively. The dimensionless saltating length and height are found to follow Pearson Type III distributions, similar to the distributions of the experimental data shown in Fig. 11. Ninety percent of the simulated saltating velocities follow a uniform distribution, which is different from the distribution of the experimental data. This is probably due to the fact that the experiments were controlled under a uniform flow condition, whereas the numerical results were analyzed based on the randomly simulated continuous saltating trajectories of a single particle.

Based on averaged values of the 60 simulation runs, three regression equations were obtained

$$SL/D = 2.428D_*^{0.27}T_*^{1.01} \tag{8}$$

$$SH/D = 0.088D_*^{0.63}T_*^{0.71} \tag{9}$$

$$SV/u_* = 3.135D_*^{0.17}T_*^{0.18} \tag{10}$$

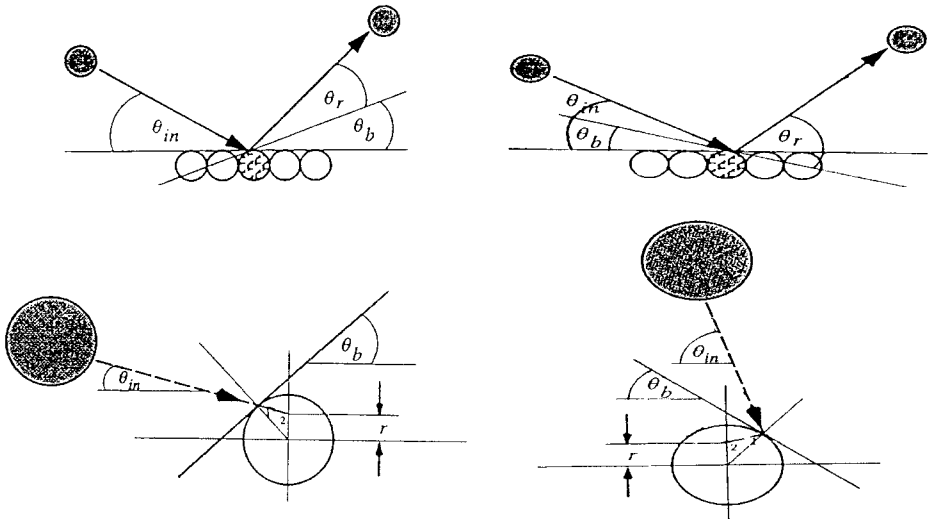

FIG. 13. Definition Sketch for Particle Collisions

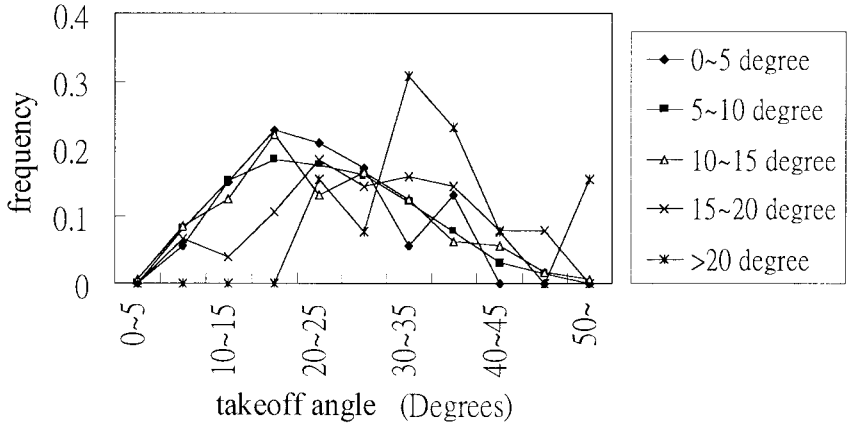

FIG. 14. Distributions of Takeoff Angles θ_{out} under Various Incidence Conditions θ_{in}

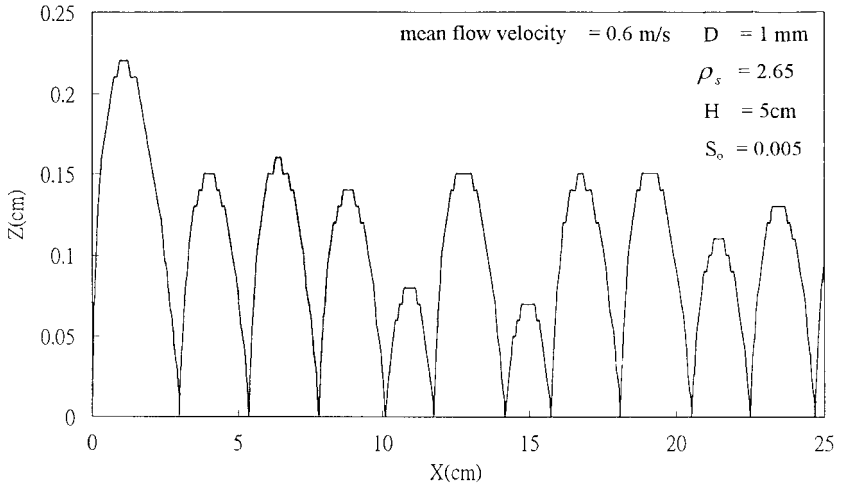

FIG. 15. Simulated Saltating Trajectories

The R'^2 values of (8)–(10) are 0.95, 0.96, and 0.97, respectively, which indicated that a good portion of the data can be adequately described by these equations.

Bed Load Equation

The bed load transport rate q_b can be calculated using the following relation:

$$q_b = C_b \times SH \times SV \tag{11}$$

where C_b = bed load concentration. Four sets of flume data conducted by Gilbert (1914), Falkner (1935), Guy et al. (1966), and Williams (1970) are analyzed in this study, and the following regression equation was obtained:

$$C_b \text{ (ppm)} = 6.19 D_*^{-0.28} T_*^{1.55} \tag{12}$$

The R'^2 value of (12) is 0.71. Substituting (9), (10), and (12) into (11), the bed load equation can thus be expressed as

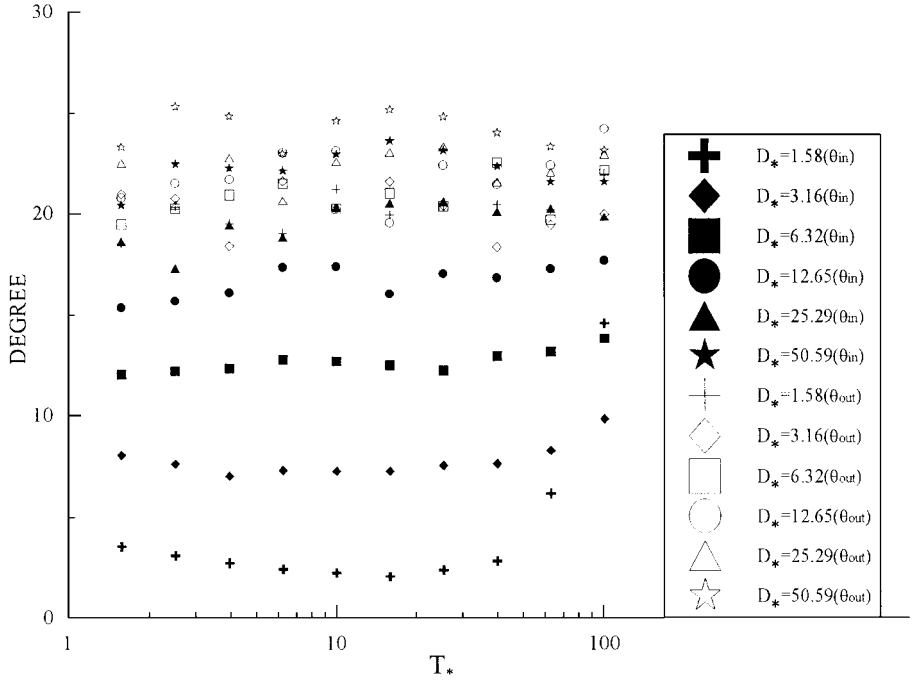

FIG. 16. Simulated Incidence Angles θ_{in} and Takeoff Angles θ_{out}

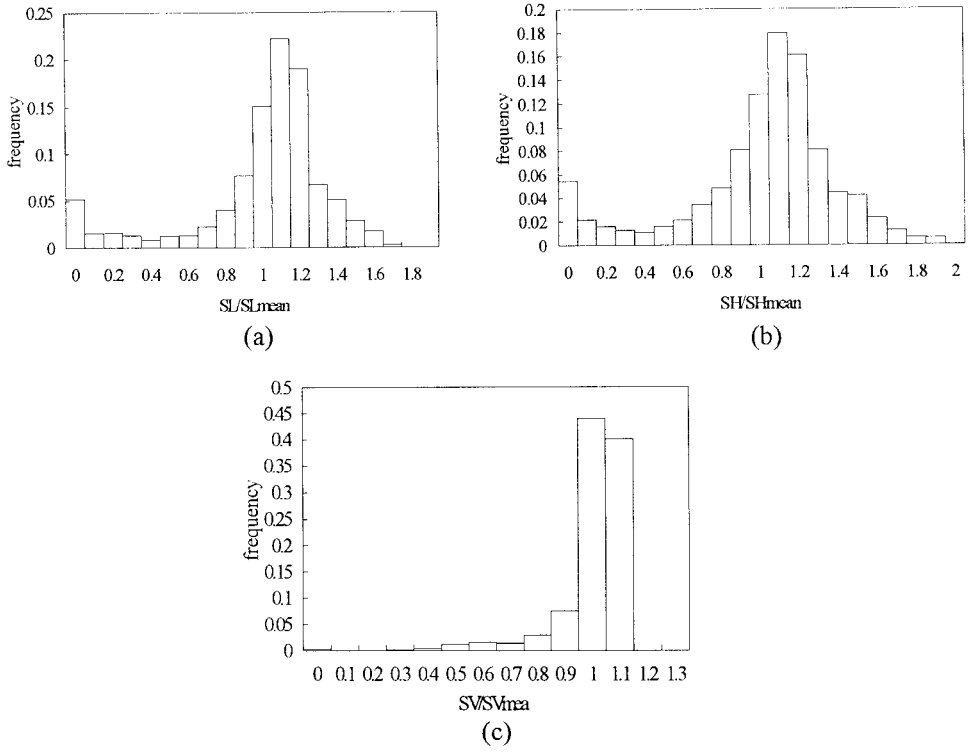

FIG. 17. Distributions of: (a) Simulated Dimensionless Saltating Lengths; (b) Heights; (c) Velocities

$$q_b(m^3/\mathrm{m}) = 1.71 d_{50} u_* D_*^{0.51} T_*^{2.44} \times 10^{-6} \qquad (13)$$

where d_{50} = mean particle size.

Comparisons of calculated and measured dimensionless sediment transport rates ($\Phi = q_b/\sqrt{\rho_s - (\rho_w/\rho_w) g d_{50}^3}$) are shown in Fig. 18. The overall accuracy is acceptable. Eq. (13) tends to slightly overestimate the bed load transport rate. This is probably due to neglect of the collisions between the saltating particles and the influence of the bed forms.

CONCLUSIONS

Particle saltation processes were investigated experimentally and numerically in this study, whose main conclusions are summarized below.

Saltation length was between 11.7 and 38.3 times particle diameter, and saltation height was between 1.35 and 2.1 times of the particle size. Average saltation velocity was about 9 to 10.6 times of u_*. Takeoff angles vary between 20° and 29°, and incidence angles were between 9° and 12°. This study also

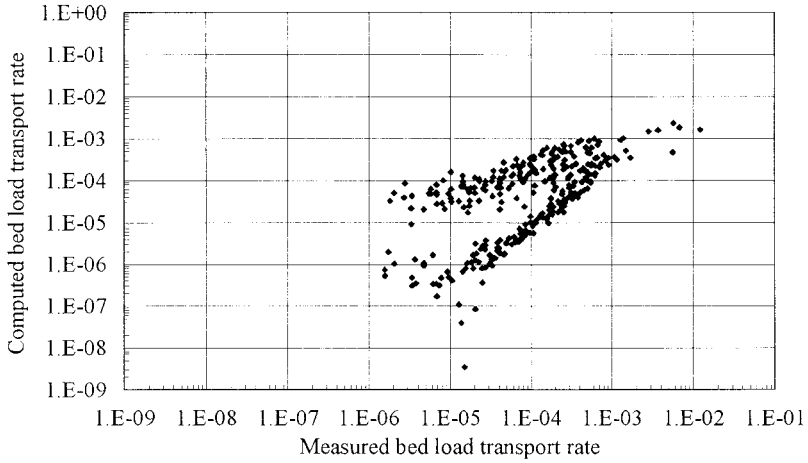

FIG. 18. Comparison of Measured and Computed Dimensionless Bed Load Transport Rates Φ [Database: Guy et al. (1966)]

found that saltation height increases with flow intensity, and corresponding variations of the saltation length are not significant.

During saltation of a coarse particle, lift force is slightly larger than drag force. Both forces are of the same magnitude when saltating particle size is small. This finding explains the difference between the saltation characteristics of a coarse and a fine particle.

When the flow parameter T_* is small, SL/D, SH/D, and SV/U_* increase with particle diameter D_*. When T_* is large, SL/D approaches a constant value for different D_*, and there will be upper limits of SH/D and SV/U_* for every D_*.

Experimental and numerical investigations show that the dimensionless saltating length and height follow Pearson Type III distributions. The measured dimensionless saltating velocity was found to follow a normal distribution, whereas the simulated dimensionless saltating velocity follows a uniform distribution.

A regression equation for bed load transport rate was obtained. This equation verified well with the flume data.

APPENDIX I. COLLISION-REBOUND MODEL OF NINO AND GARCIA

The definition sketch of the model is given in Fig. 14. The model assumes the channel bed is formed by uniformly packed spheres and a saltating particle approaching the bed at an angle θ_{in} strikes the surface that faces upstream with an angle θ_b. The striking velocity is reduced after the collision. Coefficients of restitution and friction, e and f, represent the reductions of the normal and tangential particle velocity components after the collision. These coefficients can be obtained by the experiments.

If the collision point is located at the surface facing upstream, the particle velocity components immediately after the collision $u_{p,out}$ and $v_{p,out}$ can be expressed in terms of the corresponding velocity components immediately before the collision $u_{p,in}$ and $v_{p,in}$ as

$$u_{p,out} = f(u_{p,in}^2 + v_{p,in}^2)^{1/2} \cos(\theta_{in} + \theta_b) \frac{\cos(\theta_r + \theta_b)}{\cos(\theta_r)} \quad (14)$$

$$v_{p,out} = f(u_{p,in}^2 + v_{p,in}^2)^{1/2} \cos(\theta_{in} + \theta_b) \frac{\sin(\theta_r + \theta_b)}{\cos(\theta_r)} \quad (15)$$

where θ_r = rebounding angle, $0 \le \theta_b \le \pi/6$ and $0 \le (\theta_b + \theta_r) \le \pi/2$.

If the collision point is located at the surface facing downstream, the equations become

$$u_{p,out} = f(u_{p,in}^2 + v_{p,in}^2)^{1/2} \cos(\theta_{in} + \theta_b) \frac{\cos(\theta_r - \theta_b)}{\cos(\theta_r)} \quad (16)$$

$$v_{p,out} = f(u_{p,in}^2 + v_{p,in}^2)^{1/2} \cos(\theta_{in} - \theta_b) \frac{\sin(\theta_r - \theta_b)}{\cos(\theta_r)} \quad (17)$$

when $0 \le \theta_{in} \le \pi/6$, $0 \le \theta_b \le \theta_{in}$, whereas when $\pi/6 \le \theta_{in} \le \pi/2$, $0 \le \theta_b \le \pi/6$ and $0 \le (\theta_r - \theta_b) \le \pi/2$.

Due to experimental difficulties, θ_b cannot be easily measured. A stochastic model was proposed (Garcia and Nino 1992) to determine the probability distribution function of θ_b. Assuming that a bed particle has a uniform probability of being impacted by saltating particles at any position, the impacting points can be mapped onto a set of values of r along a vertical line passing through the center of a bed particle. Thus, the values of r also follow the same uniform distribution function. With θ_{in} and r given, θ_b can be determined through a geometric transformation; that is

$$\theta_b = \cos^{-1}\left(\frac{r}{R}\cos\theta_{in}\right) - \theta_{in} \quad (18)$$

$$\theta_r = \tan^{-1}\left(\frac{e}{f}\tan(\theta_{in} + \theta_b)\right) \quad (19)$$

when $0 \le \theta_b \le \pi/6$ and $0 \le (\theta_b + \theta_r) \le \pi/2$

$$\theta_b = \theta_{in} - \sin^{-1}\left(\frac{r}{R}\cos\theta_{in}\right) \quad (20)$$

$$\theta_r = \tan^{-1}\left(\frac{e}{f}\tan(\theta_{in} - \theta_b)\right) \quad (21)$$

when $0 \le \theta_{in} \le \pi/6$, $0 \le \theta_b \le \theta_{in}$, whereas when $\pi/6 \le 0_{in} \le \pi/2$, $0 \le \theta_b \le \pi/6$ and $0 \le (\theta_r - \theta_b) \le \pi/2$, and where R = radius of the particles that form the channel bed.

ACKNOWLEDGMENTS

This study was supported by the National Science Council of Taiwan. The writers would like to thank the staff of the Hydraulic Research Laboratory of National Taiwan University for their support in conducting the experiments.

APPENDIX II. REFERENCES

Abbott, J. E., and Francis, J. R. C. (1977). ''Saltation and suspension trajectories of solid grains in a water stream.'' *Proc., Royal Soc.*, London, 284A, 225–254.

Anderson, R. S., and Hallet, B. (1986). ''Sediment transport by wind.'' *Geological Soc. of Am. Bull.*, 97.

Einstein, H. A. (1942). ''Formula for the transportation of bed-load.'' *Trans. ASCE*, 107.

Einstein, H. A. (1950). ''The bed-load function for sediment transport in open channel flows.'' *Tech. Bull. No. 1026*, U.S. Department of Agriculture, Soil Conservation Service.
Einstein, H. A., and El-Sammi, E. A. (1949). ''Hydrodynamic forces on a rough wall.'' *Rev. Modern Phys.*, 21(3), 520–524.
Falkner, H. (1935). ''Studies of river bed materials and their movement with special reference to the lower Mississippi River,'' Paper 17, U.S. Waterways Experiment Station, Vicksburg, Miss.
Francis, J. R. D. (1973). ''Experiments on the motion of solitary gains along the bed of a water stream.'' *Proc., Royal Soc.*, London, 332A, 443–471.
Garcia, M., and Nino, Y. (1992). ''Lagragian description of bedload transport by saltating particles.'' *Proc., 6th IAHR Int. Symp. on Stochastic Hydr.*, IAHR, Delft, The Netherlands, 259–266.
Gilbert, G. K. (1914). ''Transportation for debris by running water.'' Profl. Paper 86, U.S. Geological Survey, Washington, D.C.
Gordon, R., Carmichael, J. B., and Isackson, F. J. (1972). ''Saltation of plastic balls in a one-dimension flume.'' *Water Resour. Res.*, 8(2), 444–459.
Guy, H. P., Simmons, D. B., and Richardson, E. V. (1966). ''Summary of alluvial channel data from flume experiments.'' Profl. Paper 462-I, U.S. Geological Survey, Washington, D.C.
Hui, Y., and Hu, E. (1991). ''Saltation characteristics of particle motions in water.'' *Shuili Xuebao*, 12, 59–64 (in Chinese).
Lee, H. Y., and Hsu, I. S. (1994). ''Investigating of saltating particle motions.'' *J. Hydr. Engrg.*, ASCE, 120(7), 831–845.
Lee, S. Y. (1993). ''Investigations of the particle saltating process near the channel bed.'' MS thesis, Dept. of Civ. Engrg., National Taiwan University, Taipei, Taiwan (in Chinese).
Murphy, P. J., and Hooshiari, H. (1982). ''Saltation in water dynamics.'' *J. Hydr. Div.*, ASCE, 108(11), 1251–1267.
Nino, Y., and Garcia, M. (1994). ''Gravel saltation. 2. Modeling.'' *Water Resour. Res.*, 30(6), 1915–1924.
Nino, Y., and Garcia, M. (1998). ''Experiments on saltation of sand in water.'' *J. Hydr. Engrg.*, ASCE, 124(10), 1014–1025.
Nino, Y., Garcia, M., and Ayala, L. (1994). ''Gravel saltation. 1. Experiments.'' *Water Resour. Res.*, 30(6), 1907–1914.
Sekine, M., and Kikkawa, H. (1992). ''Mechanics of saltating grains. II.'' *J. Hydr. Engrg.*, ASCE, 118(4), 536–558.
Swamee, P. K., and Ojha, C. S. P. (1991). ''Drag coefficient and fall velocity of nonspherical particles.'' *J. Hydr. Engrg.*, ASCE, 117(5), 660–667.
Van Rijn, L. C. (1984). ''Sediment transport, Part I: Bed load transport.'' *J. Hydr. Engrg.*, ASCE, 110(10), 1431–1456.
Wiberg, P. L., and Smith, J. D. (1985). ''A theoretical model for saltating grains in water.'' *J. Geophys. Res.*, 91(c4), 7341–7354.
Wiberg, P. L., and Smith, J. D. (1987). ''Calculation of the critical shear stress for motion of uniform and heterogeneous sediments.'' *Water Resour. Res.*, 1471–1480.
Wiberg, P. L., and Smith, J. D. (1989). ''Model for calculating bed load transport of sediment. *J. Hydr. Engrg.*, ASCE, 115(1), 101–123.
Williams, P. G. (1970). ''Flume width and water depth effects in sediment transport experiments.'' Profl. Paper, U.S. Geological Survey, Washington, D.C., 562-H, H5.

APPENDIX III. NOTATION

The following symbols are used in this paper:

A = cross-sectional area of particle perpendicular to flow direction;
C_b = bed load concentration;
C_D = drag coefficient;
C_L = lift coefficient;
C_m = virtual mass coefficient;
D = saltating particle size;
D_b = size of particles that form channel bed;
D_* = particle dimensionless parameter;
d_{50} = mean particle size;
e = restitution coefficient;
F_G = submerged weight;
F_L, F_D = lift force and drag force, respectively;
f = friction coefficient;
g = gravitational acceleration;
H = water depth;
m = particle total mass;
q_b = bed load transport rate;
R = radius of particles that form channel bed;
R = fluid Reynolds number;
R' = correlation coefficient;
R_* = particle Reynolds number;
r = as shown in Fig. 18;
S_G = specific gravity;
S_0 = channel slope;
SL, SH, SV = saltating length, height, and velocity, respectively;
SH_{mean} = mean saltating height;
SL_{mean} = mean saltating length;
SV_{mean} = mean saltating velocity;
T^* = parameter of flow transport capacity;
u = flow velocity;
$u_{p,\text{in}}$ = particle horizontal velocity before collision;
$u_{p,\text{out}}$ = particle horizontal velocity after collision;
u_r = relative velocity;
u_{rB} = relative velocity at bottom of particle;
u_{rT} = relative velocity at top of particle;
u_* = shear velocity;
u_{*c} = critical shear velocity;
$v_{p,\text{in}}$ = particle vertical velocity before collision;
$v_{p,\text{out}}$ = particle vertical velocity after collision;
x, z = longitudinal and vertical distance, respectively;
$\dot{x}$, $\dot{z}$ = longitudinal and vertical components of particle velocity, respectively;
$\ddot{x}$, $\ddot{z}$ = longitudinal and vertical components of particle acceleration, respectively;
α_1 = coefficient of initial longitudinal component of liftoff velocity;
α_2 = coefficient of initial vertical component of liftoff velocity;
βD^2 = projected area perpendicular to flow direction;
ε = particle surface roughness;
θ = dimensionless shear stress;
θ_b = as shown in Fig. 18;
θ_{in} = impacting angle (incident angle);
θ_{out} = takeoff angle;
θ_r = rebounding angle;
μ = dynamic viscosity;
ν = kinematic viscosity;
ρ_s = specific gravity of saltating particle;
ρ_w = specific gravity of water;
Φ = dimensionless sediment transport rate; and
ϕ = channel-bed angle.